

Heterogeneous & Homogeneous & Bio- & Nano-

CHEM**CAT**CHEM

CATALYSIS

Accepted Article

Title: On the impact of hydrophobic organohybrid silicas on the stability of Ni₂P catalyst phase in the HDO of biophenols

Authors: Michael Dierks, Zhengwen Cao, Jinesh C. Manayil, Jeganathan Akilavasan, Karen Wilson, Ferdi Schueth, and Roberto Rinaldi

This manuscript has been accepted after peer review and appears as an Accepted Article online prior to editing, proofing, and formal publication of the final Version of Record (VoR). This work is currently citable by using the Digital Object Identifier (DOI) given below. The VoR will be published online in Early View as soon as possible and may be different to this Accepted Article as a result of editing. Readers should obtain the VoR from the journal website shown below when it is published to ensure accuracy of information. The authors are responsible for the content of this Accepted Article.

To be cited as: *ChemCatChem* 10.1002/cctc.201702001

Link to VoR: <http://dx.doi.org/10.1002/cctc.201702001>

WILEY-VCH

www.chemcatchem.org



On the impact of hydrophobic organohybrid silicas on the stability of Ni₂P catalyst phase in the HDO of biophenols

Michael Dierks,^a Zhengwen Cao,^a Jinesh C. Manayil,^b Jeganathan Akilavasan,^a Karen Wilson,^d

Ferdi Schüth^{a,*} and Roberto Rinaldi^{c,*}

a. Max-Planck-Institut für Kohlenforschung, Kaiser-Wilhelm-Platz 1, 45470 Mülheim-an-der-Ruhr, Germany.

b. European Bioenergy Research Institute, School of Engineering & Applied Science, Aston University, Birmingham B4 7ET, UK

c. Department of Chemical Engineering, South Kensington Campus, Imperial College London, London, SW7 2AZ, UK

d. School of Science, RMIT University, 124 La Trobe St, Melbourne VIC 3000, Australia

*corresponding authors: Ferdi Schüth, e-mail: schueth@kofo.mpg.de and Roberto Rinaldi, e-mail: rrinaldi@imperial.ac.uk.

Abstract

Hydrodeoxygenation (HDO) of lignocellulose-derived pyrolysis oils offers a process option to produce fuel substitutes. However, catalyst deactivation and stability remain a significant issue. Herein, the dependence of stability and activity of $\text{Ni}_2\text{P}/\text{SiO}_2$ HDO catalysts on the support surface polarity is addressed in detail. The support surface polarity was adjusted by copolymerizing tetraethyl orthosilicate (TEOS) with different types and amounts of organosilanes via a sol-gel process in the presence of nickel nitrate and citric acid. After thermal treatment under an inert atmosphere, Ni/SiO_2 precursors were formed. They were converted into $\text{Ni}_2\text{P}/\text{SiO}_2$ catalysts by using NaH_2PO_2 as a PH_3 source. The catalyst surface polarity was characterized by inverse gas chromatography measurements of the adsorption free energy of methanol, and specific and dispersive surface energies from polar and nonpolar probe molecule adsorption. The correlation between catalyst performance and support surface polarity indicates that, to prevent deactivation of the catalyst by water under reaction conditions, the affinity of the support towards polar substances must be decreased below a threshold value.

Introduction

High-energy density biofuels produced from the hydrodeoxygenation (HDO) of lignocellulose-derived pyrolysis products are considered as renewable and CO₂-neutral alternatives to petroleum-derived fuels (e.g. gasoline, kerosene and diesel).^{1, 2} However, the high-oxygen content of pyrolysis oils results in poor combustion properties, low stability upon storage and immiscibility with fossil crude oils. These properties hamper the drop-in utilization of pyrolysis oil as a fuel.³ Accordingly, a hydrodeoxygenation step is required, in which the oxygenated functional groups are removed by reductive processes, generating water as a byproduct. Moreover, pyrolysis oils may also contain up to 50 wt% water. Hence, the inevitable presence of water in the reaction medium usually leads to deleterious changes in the catalysts under the severe HDO conditions.⁴⁻⁸

Catalyst deactivation during hydrotreating of pyrolysis oils may occur through several pathways. One of the major pathways for catalyst deactivation is coke formation, which can be suppressed by using neutral supports (e.g. SiO₂) instead of highly acidic materials.⁹ Also, in the case of metal carbides, sulfides, nitrides or phosphides active phase oxidation can present an issue, due to their strong affinity towards oxygen.¹⁰ Traditional metal sulfide catalysts are known to suffer from deactivation during HDO in the presence of water by partial oxidation of the nickel sulfide phase.¹¹ To circumvent the problem of partial oxidation of active sites, it was demonstrated that water-sensitive active sites could be protected against deactivation during HDO by adjustment of the catalyst's surface polarity.^{12, 13}

Tailoring the surface polarity has been demonstrated to exert a significant impact on the catalytic performance for a variety of reactions.¹⁴ Notably, the adjustment of surface polarity can have a crucial influence on activity and selectivity for oxidation reactions of organic compounds using peroxides.¹⁵⁻¹⁷ Moreover, sulfonic acid groups anchored on silicas, with different polarity, showed an improved activity and stability for esterification reactions using hydrophobic

catalysts.^{18, 19} Also in metal-catalyzed reactions, e.g. dehydrogenative coupling of organosilanes and hydrogenation of hydrophobic substrates, catalysts show increased activities when the catalyst surface hydrophobicity was modified.²⁰⁻²² Also, in the field of biomass conversion, several examples have been reported on how the control of catalyst surface polarity can be beneficial for the effective valorization of biomass. In this context, quantitative conversion of fructose to HMF, without any side products, was achieved when a superhydrophobic solid acid was used as a catalyst. Such a superior performance was not achieved by using sulfuric acid or Amberlyst-15 as the acid catalyst.²³

Catalysts stability during biomass valorization can also be improved by adjustment of the catalyst surface polarity. This especially holds true for the catalytic upgrading of pyrolysis bio-oil where, as already mentioned, the catalyst stability constitutes a central problem due to the harsh reaction conditions and presence of water, which is inherent to the bio-oil or is formed during the reaction. Zapata *et al.* showed that HY zeolites modified with hydrophobic organosilanes showed improved stability in hot water ($T > 150^{\circ}\text{C}$) for cresol alkylation and alcohol dehydration and can be used for refining of biomass-derived pyrolysis oil.²⁴ Moreover, the water tolerance of propyl sulfonic acid SBA-15 catalysts, employed in esterification of pyrolysis bio-oil as a pretreatment step, was improved by co-functionalization with octyl groups.²⁵

In this contribution, we present a systematic study of the impact support polarity on the activity and stability of the Ni_2P catalyst phase in the HDO of model compounds for pyrolysis oils. Ni_2P supported on silica was chosen as a model system, since it is known to show good HDO activity, yet due to the hydrophilic character of silica, these catalysts show strong deactivation by oxidation processes involving water.^{26, 27} Model catalysts were prepared using a modified sol-gel approach, in which the polarity of the final catalyst can be adjusted by copolymerization of tetraethyl orthosilicate (TEOS) with different types and amounts of organosilanes, in the presence

of nickel nitrate and citric acid. After thermal treatment under an inert atmosphere, the obtained Ni/SiO₂ catalysts were converted into the corresponding Ni₂P phase via phosphidation with PH₃ generated by thermal decomposition of NaH₂PO₂. Recycling experiments performed using guaiacol as a substrate revealed that it is possible to stabilize the catalyst against water deactivation by copolymerizing TEOS with 50 mol% methyltriethoxysilane (MTES). The improved catalyst stability correlates well with its surface polarity properties. In fact, the best catalyst exhibited the lowest free energy of methanol adsorption, as determined by inverse gas chromatography (IGC).

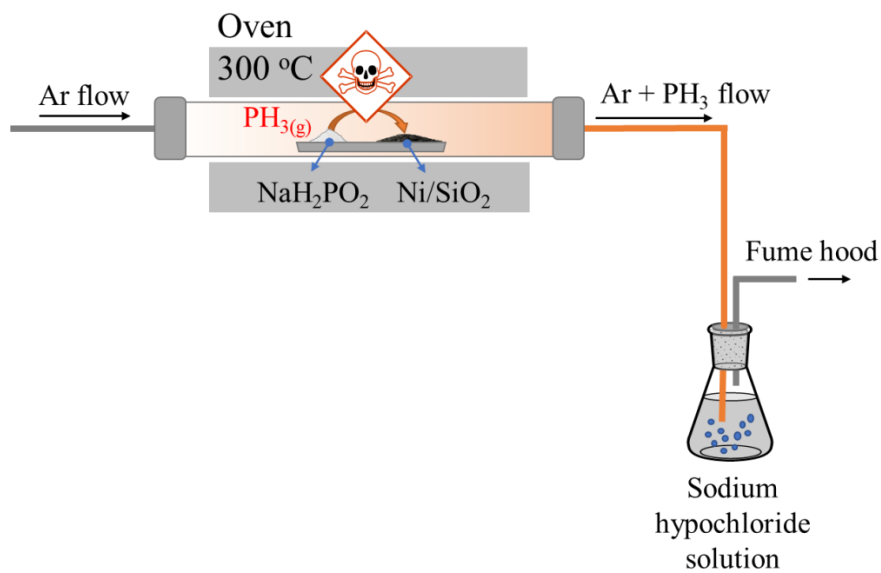
Results and discussion

Characterization of the catalysts

To explore the influence of the catalyst hydrophobicity on the HDO performance of Ni₂P/SiO₂ catalysts, a series of different model catalysts was prepared by acid-catalyzed co-condensation of TEOS with different types and various quantities of organic functions (denoted as 'R', Table 1). Ni supported on organohybrid silica supports were prepared by modifying a sol-gel synthesis procedure reported by Takahashi *et al.*²⁸ For the preparation of the unmodified Ni/SiO₂ catalyst, TEOS was employed as the silica source, nickel nitrate hexahydrate as the Ni source, and citric acid monohydrate as an organic additive. In the synthesis, citric acid (CA) is responsible for the formation of mesopores. Furthermore, CA helps to increase the dispersion of the Ni particles. To initiate the hydrolysis and condensation of the silica precursors a 0.25 mol L⁻¹ nitric acid solution was added to the system.^{28, 29} Employing methyltriethoxysilane (MTES), a transparent green colored gel with an R:Si ratio of up to 0.5 could be prepared. However, when ethyltriethoxysilane (ETES) or octyltriethoxysilane (OTES) were used, no clear (green) gel was obtained at a R:Si ratio of 0.5. In these cases, transparent green gels were obtained at R:Si ratios of 0.2 (for ETES) and 0.05 (for OTES). Utilizing phenyltriethoxysilane (PTES) as the organosilane, a transparent green

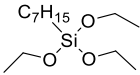
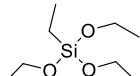
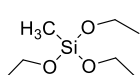
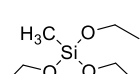
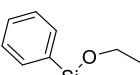
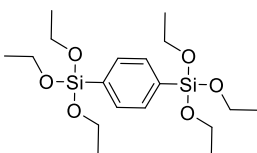
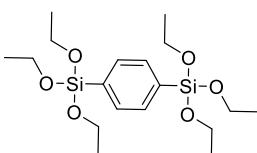
gel could be produced at an R:Si ratio of 0.1. Employing 1,4-bis(triethoxysilyl)benzene (BTSEB), the R:Si ratio could be further increased to an R:Si ratio of 0.5, while a transparent green colored gel was obtained.

As will be discussed in a greater deal of detail later in this section, the gels were converted into Ni/SiO₂ precursors by thermal treatment under an Argon flow. First, the gels were heated to 170 °C for 1.5 h and, sequentially, to 400 °C for 2 h using a heating ramp of 100 °C h⁻¹. Ni/SiO₂ precursor prepared using TEOS presents a 33 wt% nominal Ni loading. All the Ni/SiO₂ precursors were then phosphided with PH_{3(g)}, generated by thermal decomposition of NaH₂PO₂ ($2 \text{ NaH}_2\text{PO}_2(\text{s}) \rightarrow \text{Na}_2\text{HPO}_4(\text{s}) + \text{PH}_3(\text{g})$). For the reaction, NaH₂PO₂ (0.8 g, located on the inlet Ar-flow side) and Ni/SiO₂ precursor (0.1 g, located on the outlet Ar-flow side) were placed separately (approximately a 1-cm distance between the powders) in a crucible, as schematically represented in Scheme 1. The system was flushed with Ar for 0.5 h and then heated to 300 °C and kept at this temperature for 1 h. The exhaust gases were bubbled through an aqueous solution of sodium hypochlorite to oxidize remaining (highly toxic) PH₃ in the gas stream. Table 1 lists the textural properties and C-content of the Ni₂P/organohybrid-SiO₂ catalysts.



Scheme 1 Experimental setup for the phosphidation of Ni/SiO₂ precursors under an atmosphere of PH₃ generated by thermal decomposition of NaH₂PO₂ at 300 °C.

Table 1. Textural properties and C-content of Ni₂P/organohybrid-SiO₂ catalysts prepared by co-condensation of TEOS with various organosilanes and phosphided with PH₃ generated by thermal decomposition of NaH₂PO₂ at 300 °C.

Material	Organosilane Monomer	R:Si	S _{BET} (m ² g ⁻¹)	Pore volume (cm ³ g ⁻¹)	Average pore size (nm)	C-content(%)		
						Expected (%)	Found (%)	Estimated by subtraction (%) ^[a]
Ni ₂ P/SiO ₂ -TEOS	-	-	465	0.53	7.3	0	8.6±0.1	-
Ni ₂ P/SiO ₂ -50TES		0.05	449	0.42	5.0	5	11.3±0.2	2.7
Ni ₂ P/SiO ₂ -20ETES		0.2	470	0.42	4.7	5	13.5±0.2	4.9
Ni ₂ P/SiO ₂ -20MTES		0.2	484	0.51	6.2	2	12.1±0.3	3.5
Ni ₂ P/SiO ₂ -50MTES		0.5	532	0.68	12.7	6	15.5±0.2	6.9
Ni ₂ P/SiO ₂ -10PTES		0.1	568	0.52	5.0	7	15.6±0.2	6.9
Ni ₂ P/SiO ₂ -20BTBSB		0.2	563	0.47	6.2	12	15.7±0.5	7.1
Ni ₂ P/SiO ₂ -50BTBSB		0.5	523	0.38	4.7	16	25.3±0.4	16.7

[a] Estimated by subtraction of the C-content of Ni₂P/SiO₂-TEOS from the other material samples

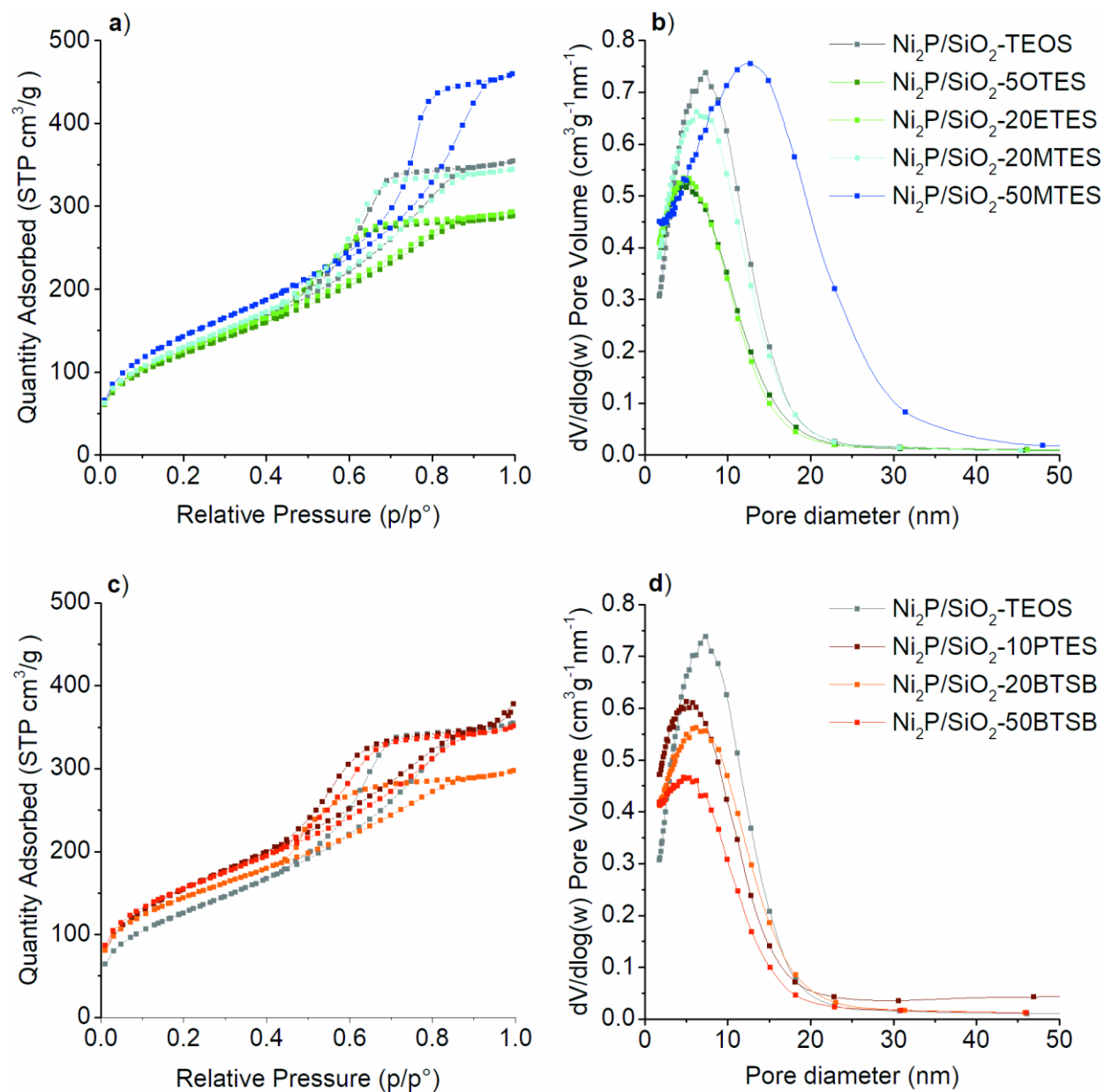


Figure 1 a) N₂ adsorption-desorption isotherms for $\text{Ni}_2\text{P}/\text{SiO}_2$ catalysts prepared using TEOS and organosilanes with alkyl groups; b) Pore size distribution for $\text{Ni}_2\text{P}/\text{SiO}_2$ catalysts prepared using TEOS and organosilanes with alkyl groups; c) N₂ adsorption-desorption isotherms for $\text{Ni}_2\text{P}/\text{SiO}_2$ catalysts prepared using TEOS and organosilanes with phenyl groups; d) Pore size distribution for $\text{Ni}_2\text{P}/\text{SiO}_2$ catalysts prepared using TEOS and organosilanes with phenyl groups.

In all cases, the isotherms are of type IV(H2), typical for mesoporous materials with complex pore structure. Specific surface areas, calculated by using the BET method (Table 1), varied between $449 \text{ m}^2 \text{ g}^{-1}$ ($\text{Ni}_2\text{P}/\text{SiO}_2\text{-50TES}$) and $568 \text{ m}^2 \text{ g}^{-1}$ ($\text{Ni}_2\text{P}/\text{SiO}_2\text{-10PTES}$), while the $\text{Ni}_2\text{P}/\text{SiO}_2\text{-TEOS}$ catalysts showed a surface area of $465 \text{ m}^2 \text{ g}^{-1}$. These results indicate that the different types and amounts of organosilane monomers exert an effect on the resulting S_{BET} of the $\text{Ni}_2\text{P}/\text{SiO}_2$ catalysts. A more significant increase in S_{BET} was obtained when copolymerizing phenyl-functionalized silanes with TEOS ($523 \text{ m}^2 \text{ g}^{-1} < S_{\text{BET}} < 568 \text{ m}^2 \text{ g}^{-1}$ vs. $465 \text{ m}^2 \text{ g}^{-1}$ for TEOS-derived material). However, the increase in S_{BET} was much less pronounced for the materials prepared by copolymerization of alkyl-functionalized silanes and TEOS ($449 \text{ m}^2 \text{ g}^{-1} < S_{\text{BET}} < 484 \text{ m}^2 \text{ g}^{-1}$). In these cases, a significant effect upon S_{BET} was only observed for the $\text{Ni}_2\text{P}/\text{SiO}_2\text{-50MTES}$ catalyst ($S_{\text{BET}} 532 \text{ m}^2 \text{ g}^{-1}$). The average pore diameter for the $\text{Ni}_2\text{P}/\text{SiO}_2\text{-TEOS}$ catalyst was determined to be 7.3 nm with a pore volume of $0.53 \text{ cm}^3 \text{ g}^{-1}$. When alkyl or phenyl-functionalized silanes were copolymerized with TEOS, the average pore size of the catalysts varied between 4.7 nm ($\text{Ni}_2\text{P}/\text{SiO}_2\text{-ETES}$) and 12.7 nm ($\text{Ni}_2\text{P}/\text{SiO}_2\text{-50MTES}$). Compared to $\text{Ni}_2\text{P}/\text{SiO}_2\text{-TEOS}$ catalysts, the pore size decreased for all the catalysts supported on organohybrid silicas. The only exception to this trend was the $\text{Ni}_2\text{P}/\text{SiO}_2\text{-50MTES}$ catalyst. For this catalyst, the pore diameter (12.7 nm) and pore volume ($0.68 \text{ cm}^3 \text{ g}^{-1}$) were both higher than for $\text{Ni}_2\text{P}/\text{SiO}_2\text{-TEOS}$ catalyst. As expected, these results imply that the incorporation of 50 mol% methyltriethoxysilane into the silica network had a main impact on the general pore structure and volume. The decrease of the pore volume and pore diameter for most of the catalysts is due to the incorporation of the organic groups and has been observed before for organic silica hybrid materials.³⁰ The increased pore volume and diameter of the $\text{Ni}_2\text{P}/\text{SiO}_2\text{-50MTES}$ catalyst, compared to the $\text{Ni}_2\text{P}/\text{SiO}_2\text{-TEOS}$ and $\text{Ni}_2\text{P}/\text{SiO}_2\text{-20MTES}$ catalyst, likely results from an alteration of the general network of the material due to the

high-content of organosilane, which can only form three bonds with other silicate moieties, in contrast to TEOS, which can be connected to other additional four silicon atoms via Si-O-Si bonds.

Table 1 reveals another important feature of the Ni₂P/SiO₂ materials. A direct quantitative determination of the amount of incorporated organic functionalities using elemental analysis is not fully feasible, due to the presence of remnant carbonaceous materials after the thermal treatment at 400 °C under Ar atmosphere, as indicated by the C-content of 8.6±0.1% found in Ni₂P/SiO₂-TEOS (Table 1). Therefore, it was only possible for us to estimate the C-content attributable to the organosilane incorporation in the organohybrid silicas. By subtraction of the C-content of Ni₂P/SiO₂-TEOS from those content of the other materials, we could verify that, apart from Ni₂P/SiO₂-20BTBSB, there is a good agreement between the estimated and expected C-content in the samples.

To examine further whether the organosilane groups are preserved after the thermal treatments, ATR-IR spectra of the phosphided materials were recorded (Figure 2). For Ni₂P/SiO₂-20MTES and Ni₂P/SiO₂-50MTES, the incorporation of methyl groups into the silica network is verified by the sharp band at around 1270 cm⁻¹, assigned to the symmetric bending vibration of CH₃ group in Si-CH₃ (Figure 2d and 2e).³¹ Logically, the signal intensity also correlates with the number of incorporated methyl groups into the network (Figure 2d and 2e). For the Ni₂P/SiO₂-20ETES catalyst (Figure 2c), the band relative to the symmetric bending vibration of the Si-CH₂ group is only present as low-intensity shoulder (at around 1260 cm⁻¹), because the IR absorption of the Si-CH₂ decreases compared to the Si-CH₃ group. For the Ni₂P/SiO₂-50TES catalyst, this band was not detected, which might be a consequence of the low amount of incorporated octyl groups and a further decrease of the absorption of the Si-CH₂-bending vibration, with increasing alkyl chain length.³¹ In turn, the ATR-IR spectra of the phenyl modified catalysts exhibit the typical absorption bands of phenyl groups between 1650-1350 cm⁻¹ (aromatic carbon stretching vibrations)

and the C-H bending vibrations at 740 cm^{-1} and 695 cm^{-1} , indicating the successful incorporation of phenyl groups into the silica network.³¹ However, in these cases, the characteristic silicon-phenyl linkage vibration, which appears at about 1120 cm^{-1} , is only present as a shoulder. This is due to overlap with the broad and intense Si-O-Si asymmetric stretch vibrations, which also appears between 1000 and 1111 cm^{-1} .³¹ Again, the intensity of the absorption bands agrees with the quantity of incorporated organic groups (i.e. the IR band intensity increased from the $\text{Ni}_2\text{P}/\text{SiO}_2\text{-10PTES}$ to the $\text{Ni}_2\text{P}/\text{SiO}_2\text{-50BTSB}$ catalyst). Finally, the absence of the characteristic IR bands related to carboxylic/carboxylate groups (e.g. for R-COOH species: an intense signal centered at about 1675 cm^{-1} ; for the carboxylate ion form (a broad band between 1320 and 1450 cm^{-1} and a signal centered at about 1530 cm^{-1})³² reveals that CA was decomposed at $400\text{ }^\circ\text{C}$ (forming a CO_2 and H_2O , and a carbonaceous material, as revealed by elemental analysis, Table 1).

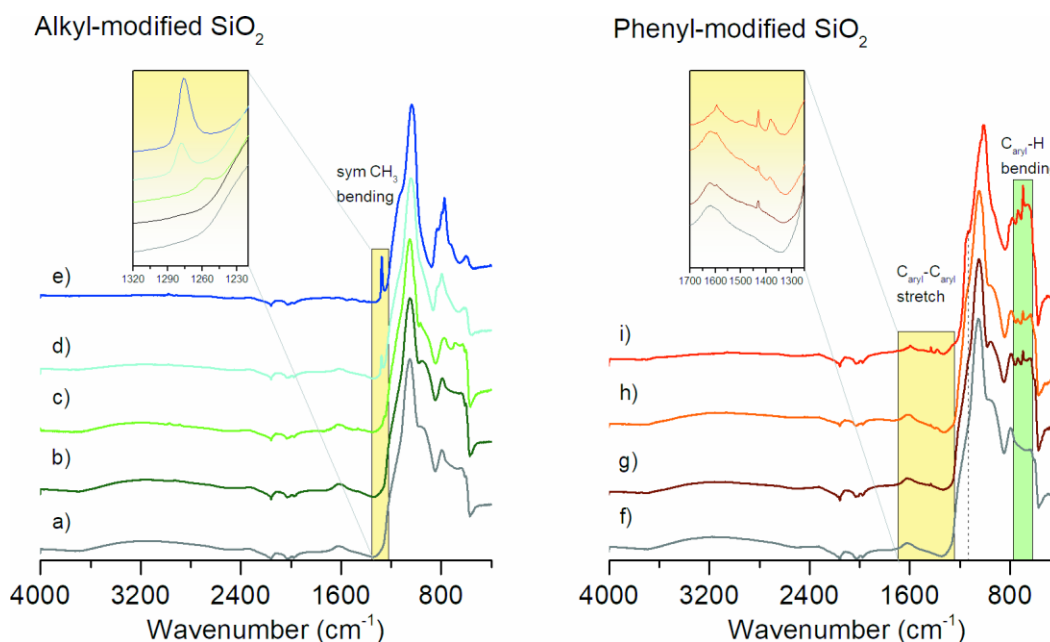


Figure 2 ATR-IR spectra of Ni_2P supported on alkyl-modified silicas: a) $\text{Ni}_2\text{P}/\text{SiO}_2\text{-TEOS}$, b) $\text{Ni}_2\text{P}/\text{SiO}_2\text{-5OTES}$, c) $\text{Ni}_2\text{P}/\text{SiO}_2\text{-20ETES}$, d) $\text{Ni}_2\text{P}/\text{SiO}_2\text{-20MTES}$, e) $\text{Ni}_2\text{P}/\text{SiO}_2\text{-50MTES}$; Ni_2P supported on phenyl-modified silicas: f) $\text{Ni}_2\text{P}/\text{SiO}_2\text{-TEOS}$, g) $\text{Ni}_2\text{P}/\text{SiO}_2\text{-10PTES}$, h) $\text{Ni}_2\text{P}/\text{SiO}_2\text{-20BTSB}$, i) $\text{Ni}_2\text{P}/\text{SiO}_2\text{-50BTSB}$

XRD patterns of the Ni/SiO₂ catalyst precursor after thermal treatment at 400 °C under Ar atmosphere (Figure 3) displays the typical (111) and (200) reflections characteristic of metallic Ni ($2\theta = 44^\circ$ and 51° , respectively, Figure 3a). This observation indicates that the reduction of Ni(II) sites in the precursor can take place without the need of a reducing atmosphere (H₂). This observation is surprising because of the stability of NiO: $\Delta_f G^\circ(\text{NiO}) = -337.64 \text{ kJ mol}^{-1}$.³³ However, it is not unique, as recently, Abu-Zied and Asiri reported a detailed study of the thermal decomposition of nickel citrate into Ni/NiO composite particles.³⁴ In that study, the conversion of NiO to Ni and O₂ occurred at 510 °C under a N₂ atmosphere. Furthermore, previous results by Dong *et al.* also demonstrated the conversion $\text{NiO}_{(s)} \rightleftharpoons \text{Ni}_{(s)} + \frac{1}{2}\text{O}_{2(g)}$ to be possible for sputtered NiO films heated under vacuum to temperatures as low as 400 °C.³⁵ Although this system differs considerably from ours, those results lend insight into possible mechanism(s) underlining the conversion of NiO into Ni, which was reported to start at the outermost surface of the film and attributed to excess Ni(II) vacancies formed during the sputtering step.³⁵ Ni(II) vacancies cause neighboring O²⁻ ions to become incompletely bonded. As a result, the decomposition of NiO films should require less stringent conditions. However, the decomposition of NiO was demonstrated to be limited to a film thickness of 100 nm.³⁵ From previous observations reported in the literature, the formation of the metallic Ni phase in our materials seems to be related to the formation of small NiO clusters upon thermal decomposition of Ni citrate/nitrate species in the gel. Importantly, it is apparent from the high C-content found in the Ni₂P/SiO₂ catalysts (Table 1) that reducing gases, hypothetically generated by partial decomposition of alkyl or aryl groups of the organohybrid silicas,³⁶ play no major role in the chemical reduction of the Ni in the material. In fact, considering that the nominal Ni loading is 33 wt%, the reduction of Ni(II) to Ni(0) would consume a substantial amount of the alkyl or aryl groups incorporated in the organohybrid silica support. Nonetheless,

this hypothesis was not verified by our results, as demonstrated by the high C-content in the samples (Table 1).

After the phosphidation of Ni/SiO₂ precursors, the typical (111), (201), (210) and (300) and (211) reflections for Ni₂P at 2θ values of 40°, 44°, 47° and 54°, respectively, were observed. This result demonstrates the successful transformation of the Ni/SiO₂ precursor into the Ni₂P/SiO₂ (Figure 3b-i). Notably, XRD patterns of the various Ni₂P/SiO₂ catalysts, supported on either pure silica or organohybrid silica supports, display no significant differences in terms of peak width, which indicates that all the Ni₂P crystallites on the support are similar in size (ca. 12-13 nm, as determined by TEM analysis).

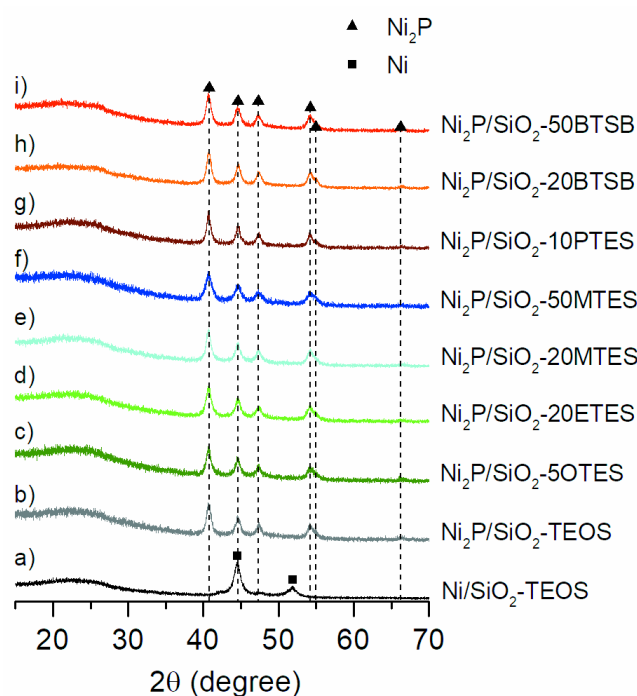


Figure 3 XRD of the Ni/SiO₂ precursor using 100% TEOS and Ni₂P/SiO₂ catalysts obtained from phosphidation of a Ni/SiO₂ precursor prepared by using different amounts and different types of organosilanes.

To provide an in-depth analysis of the Ni₂P phase in the Ni₂P/SiO₂-TEOS (benchmark catalyst) and the Ni₂P/SiO₂-50MTES (best catalyst, as will be presented later), HR-TEM images of the Ni₂P/SiO₂-TEOS and the Ni₂P/SiO₂-50MTES catalysts were collected (Figure 4). By

inspection of the HR-TEM images, no significant difference between the two catalysts was observed, as indicated by the histograms in Figure 4a and 4d. The average particle size for the $\text{Ni}_2\text{P}/\text{SiO}_2\text{-TEOS}$ and $\text{Ni}_2\text{P}/\text{SiO}_2\text{-50MTES}$ catalysts, determined by evaluating 200 particles for each catalyst, were found to be 13.6 ± 4.4 nm and 12.4 ± 3.9 nm, further supporting the statement that there is no significant difference in terms of Ni_2P particle size between the two catalysts.

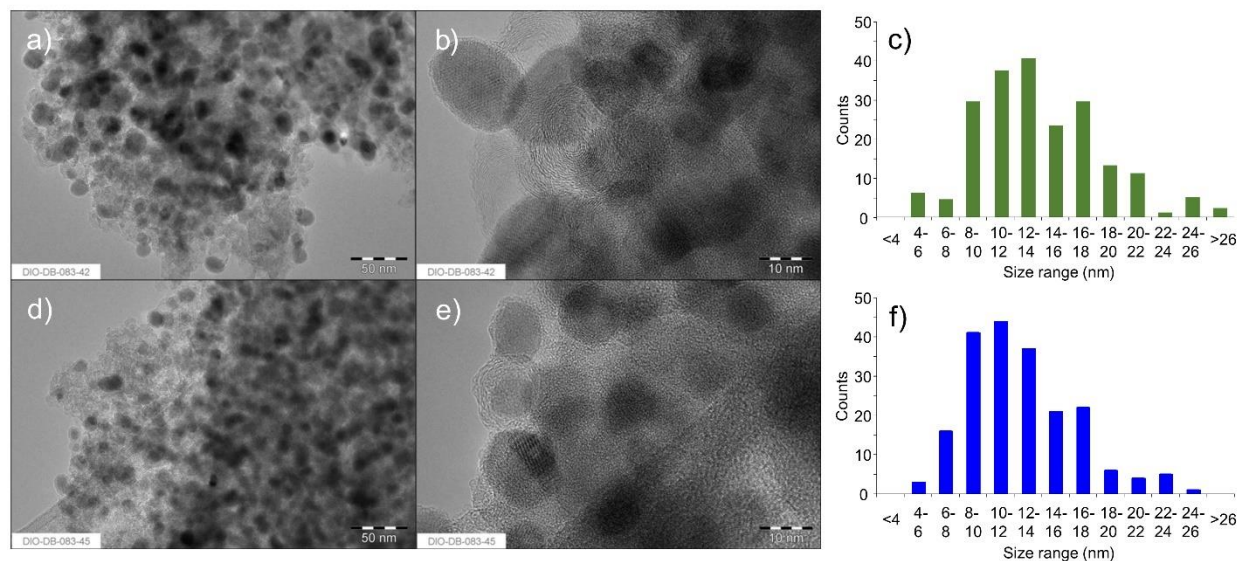


Figure 4 a, b correspond to TEM images of $\text{Ni}_2\text{P}/\text{SiO}_2\text{-TEOS}$ catalyst; d, e TEM images of $\text{Ni}_2\text{P}/\text{SiO}_2\text{-50MTES}$; c) and f) display the particle size distribution determined by evaluating the size of 200 nanoparticles.

In this section, it was demonstrated that $\text{Ni}_2\text{P}/\text{SiO}_2$ materials were successfully synthesized. Furthermore, HR-TEM images of selected samples show that there are no significant differences in terms of the particles size and distribution of the particles on the support. Nitrogen sorption isotherms show that incorporation of phenyl groups into the framework results in a slight increase of the S_{BET} , while for the alkyl-modified catalyst the surface area decreases slightly with the only exception of the $\text{Ni}_2\text{P}/\text{SiO}_2\text{-50MTES}$ catalyst, for which S_{BET} increases slightly, compared to the $\text{Ni}_2\text{P}/\text{SiO}_2\text{-TEOS}$ catalyst. Also with respect to the pore volume and pore diameter, the $\text{Ni}_2\text{P}/\text{SiO}_2\text{-50MTES}$ catalyst does not fit the general trend. For all the organically modified catalysts the pore

volume and pore diameter decreased, compared to the $\text{Ni}_2\text{P}/\text{SiO}_2\text{-TEOS}$ catalyst. In contrast to this, for the $\text{Ni}_2\text{P}/\text{SiO}_2\text{-50MTES}$, the pore volume increases from $0.53 \text{ cm}^3 \text{ g}^{-1}$ ($\text{Ni}_2\text{P}/\text{SiO}_2\text{-TEOS}$) to $0.68 \text{ cm}^3 \text{ g}^{-1}$ ($\text{Ni}_2\text{P}/\text{SiO}_2\text{-50MTES}$), and the pore diameter increases from 7.3 nm ($\text{Ni}_2\text{P}/\text{SiO}_2\text{-TEOS}$) to 12.7 nm ($\text{Ni}_2\text{P}/\text{SiO}_2\text{-50MTES}$). These results suggest that for the $\text{Ni}_2\text{P}/\text{SiO}_2\text{-50MTES}$ the number of organosilanes introduced into the framework changes the structure of the material compared to the unmodified one. This is likely due to the different bonding possibilities of the organosilanes, resulting in a more open structure. Most importantly, elemental analysis and ATR-IR spectroscopy of the samples provide firm evidence that there is a successful incorporation of different amounts of methyl and phenyl groups into the silica network, which remained in the structured even after thermal treatment at 400 °C under Ar flow.

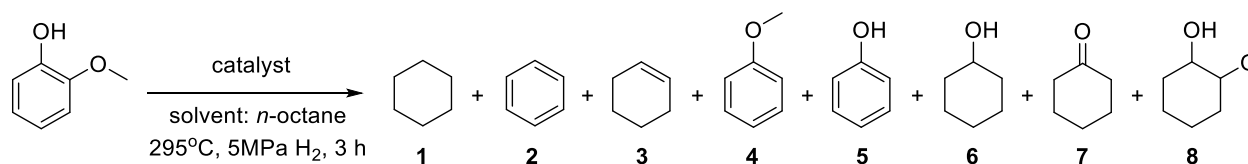
Catalyst tests

For the catalyst test, we chose the HDO of guaiacol as the model reaction (at 295 °C and 5 MPa H_2 pressure for 3 h). Using the $\text{Ni}_2\text{P}/\text{SiO}_2\text{-TEOS}$ catalyst (Table 2, entry 1, benchmarking catalyst), a 69% conversion was achieved. The main products of the reaction are cyclohexane formed with a 36% yield and benzene with a 17% yield. Cyclohexene was obtained only in minor quantities (<1% yield). Besides fully deoxygenated products, also partially deoxygenated aromatic and aliphatic products were found. As oxygenated aromatic compounds, anisole and phenol were observed with 9% and 5% yields, respectively. As aliphatic oxygenates, cyclohexanol, cyclohexanone and 2-methoxycyclohexanol were formed, but in minor quantities (yields lower than 1%).

Ni_2P catalysts supported on organohybrid silicas modified with alkyl groups (Table 2, entry 2-5), showed a decrease in activity by approximately 20%, compared to the benchmarking catalyst $\text{Ni}_2\text{P}/\text{SiO}_2\text{-TEOS}$. The main products of the reactions are still cyclohexane and benzene. Notably, an increase (by a factor of 2.5) in the amount of methylsilane groups incorporated in the silica had

no effect on the reaction outcome (Table 2, entry 4 and 5). Furthermore, substitution of methyl by ethyl or octyl groups, while the R:TEOS ratio is kept at 0.2 or 0.05 (Table 2 entry 2 and 3), did not alter the results. From this, it can be concluded that incorporation of alkyl functional groups into the silica network decreased the activity for guaiacol HDO reactions, compared to $\text{Ni}_2\text{P}/\text{SiO}_2\text{-TEOS}$. Strikingly, Ni_2P catalysts supported on organohybrid silicas modified with phenyl groups (Table 2 entry 6, 7, and 8) show an activity similar to that of $\text{Ni}_2\text{P}/\text{SiO}_2\text{-TEOS}$ catalyst. Interestingly, irrespective of the nominal quantity of incorporated phenyl groups, the conversion is not further improved above 67%. In terms of product yields, $\text{Ni}_2\text{P}/\text{SiO}_2\text{-10PTES}$ presents an identical profile to the benchmarking catalyst. Therefore, considering the (similar) catalyst performance, we chose to focus our study on $\text{Ni}_2\text{P}/\text{SiO}_2\text{-TEOS}$, $\text{Ni}_2\text{P}/\text{SiO}_2\text{-20BTBS}$ and $\text{Ni}_2\text{P}/\text{SiO}_2\text{-50MTES}$ catalyst, which presented the most distinguished features in the series.

Table 2. Catalytic results for guaiacol HDO using Ni_2P catalysts supported on pure silica or silica modified with different types and amounts of organic functional groups.



entry	catalyst	Conversion (%)	Yield (%)							
			deoxygenated products		aromatic oxygenates		aliphatic oxygenates		7	8
			1	2	3	4	5	6		
1	$\text{Ni}_2\text{P}/\text{SiO}_2\text{-TEOS}$	69	36	17	<1	9	5	<1	<1	<1
2	$\text{Ni}_2\text{P}/\text{SiO}_2\text{-5OTES}$	43	16	13	<1	8	5	<1	<1	<1
3	$\text{Ni}_2\text{P}/\text{SiO}_2\text{-20ETES}$	40	15	11	<1	8	5	<1	<1	<1
4	$\text{Ni}_2\text{P}/\text{SiO}_2\text{-20MTES}$	49	22	11	<1	8	6	<1	<1	<1
5	$\text{Ni}_2\text{P}/\text{SiO}_2\text{-50MTES}$	49	23	12	<1	8	5	<1	<1	<1

6	Ni ₂ P/SiO ₂ -10PTES	67	35	16	<1	9	6	<1	<1	<1
7	Ni ₂ P/SiO ₂ -20BTBSB	69	43	13	<1	8	5	<1	<1	<1
8	Ni ₂ P/SiO ₂ -50BTBSB	66	42	12	<1	7	4	<1	<1	<1

Effects of support polarity on catalyst activity

To put the current results into a broader context, the general nature of pyrolysis oils must be considered. While fossil crude oils are considered as nonpolar, due to their low oxygen content, pyrolysis oils can be considered as polar and, therefore, hydrophilic. This is a direct consequence of the high oxygen content in pyrolysis oils, present in the form of different acids, aldehydes, esters, alcohols, ethers, ketones, phenolics, sugars, furans, and up to 50 wt% water.^{37, 38} In this manner, adjusting catalyst polarity should exert a direct effect on the interaction between catalyst and substrate. To characterize the interactions of the prepared catalysts with the polar constituents of pyrolysis oils, the free energy of methanol adsorption ($-\Delta G_{ads}^{SP}(MeOH)$) and surface energies were determined, using inverse gas chromatography (IGC) for Ni₂P/SiO₂-TEOS, Ni₂P/SiO₂-20BTBSB and Ni₂P/SiO₂-50MTES catalysts (Table 3). IGC is a powerful technique to determine the surface properties associated with catalytic materials (details given in experimental section) and it gives information on physical (dispersive) and chemical (specific/polar) interactions through the adsorption of alkanes and polar probe molecules, respectively.²⁵ Dispersive surface energy provides insight into the surface hydrophobicity, higher the value of dispersive surface energy, higher the hydrophobic character.^{39, 40} In turn, the surface polarity (hydrophilicity) can be directly correlated with the free energy of adsorption of polar probe molecules and specific surface energy. Owing to detection and analysis difficulties while working with water as a probe molecule in IGC (i.e. flame ionization detector, FID, cannot detect water), methanol was taken as a substitute for free energy calculations. The dispersive surface energy (γ_S^D) was determined as a measure of the

organophilicity of the catalyst. Among the three catalysts, the Ni₂P/SiO₂-50MTES catalyst displayed the lowest $-\Delta G_{ads}^{SP}(MeOH)$ value of 10.5 kJ mol⁻¹, compared to 15.0 kJ mol⁻¹ and 17.8 kJ mol⁻¹ for the Ni₂P/SiO₂-TEOS and Ni₂P/SiO₂-20BTBSB catalyst, respectively. Considering the dispersive surface energy, the Ni₂P/SiO₂-20BTBSB catalyst displayed the highest value of 80 mJ m⁻². Interestingly, the dispersive surface energies for the Ni₂P/SiO₂-TEOS and Ni₂P/SiO₂-50MTES catalysts, which were determined to be 47 mJ m⁻² and 50 mJ m⁻², are very similar, in spite of the presence of methyl groups, in the case of the Ni₂P/SiO₂-50MTES catalyst. With higher dispersive surface energy, Ni₂P/SiO₂-20BTBSB possesses the most hydrophobic character among the three catalysts. Literature validates dispersive surface energy as a measure of hydrophobicity of materials, with carbons samples with more hydrophobic character possessing high dispersive surface energy >150 mJ m⁻²,^{41, 42} while hydrophilic silica^{41, 42} and cellulose^{25, 39, 41, 43, 44} exhibit lower values ~ 50 mJ m⁻² and ~ 40 mJ m⁻², respectively. Hence, Ni₂P/SiO₂-20BTBSB which exhibits dispersive surface energy of 80 mJ m⁻² should be more hydrophobic than Ni₂P/SiO₂-TEOS (47 mJ m⁻²) and Ni₂P/SiO₂-50MTES (50 mJ m⁻²).

Table 3 Free energies of methanol adsorption ($-\Delta G_{ads}^{SP}(MeOH)$) and dispersive surface energies (γ_S^D) for the Ni₂P/SiO₂-TEOS, Ni₂P/SiO₂-20BTBSB, Ni₂P/SiO₂-50BTBSB, Ni₂P/SiO₂-20MTES and Ni₂P/SiO₂-50MTES catalysts, measured using inverse gas chromatography.

Sample	Inverse gas chromatography measurements	
	$-\Delta G_{ads}^{SP} (MeOH) [kJ mol^{-1}]$	$\gamma_S^D [mJ m^{-2}]$
Ni ₂ P/SiO ₂ -TEOS	15.0	47
Ni ₂ P/SiO ₂ -20BTBSB	17.8	80
Ni ₂ P/SiO ₂ -50BTBSB	13.9	82
Ni ₂ P/SiO ₂ -20MTES	13.0	51
Ni ₂ P/SiO ₂ -50MTES	10.5	50

The interactions of the modified catalysts with a typical polar constituent of pyrolysis oils were exemplified using guaiacol as an example Figure 5a. As already discussed above, modification of the catalyst with methyl groups decreased the activity for guaiacol HDO from 65±5%, for the Ni₂P/SiO₂-TEOS catalyst, to 46±4% for the Ni₂P/SiO₂-50MTES catalyst. In contrast, the conversion of the Ni₂P/SiO₂-20BTBSB catalyst, modified with phenyl groups, was found to be 67±3%, and hence did not decrease compared to the Ni₂P/SiO₂-TEOS catalyst (Figure 5a). This correlates with the free energies of methanol adsorption, which are higher for the Ni₂P/SiO₂-TEOS and Ni₂P/SiO₂-20BTBSB catalysts, compared to the Ni₂P/SiO₂-50MTES catalyst. The modification of the catalyst with alkyl groups reduced the catalyst affinity towards polar constituents of pyrolysis oils (e.g. guaiacol), compared to unmodified or phenyl group modified catalysts. However, despite the fact that phenyl groups are hydrophobic, they are capable of establishing strong π - π interactions⁴⁵ with the phenolic components present in pyrolysis oils. Therefore, this type of interaction appears to be vital to sustaining the conversion at the levels as high as that found for the hydrophilic Ni₂P/SiO₂-TEOS catalyst.

HDO of the nonpolar bio-oil model compound diphenyl ether was performed to confirm the assumption that the affinity of the catalyst towards less polar bio-oil compounds can be characterized by their dispersive surface energy. Evidently, the catalytic results correlate well with the dispersive surface energies of the three catalysts (Table 3). Thus, the $\text{Ni}_2\text{P}/\text{SiO}_2\text{-20BTBSB}$ catalyst, which has the highest dispersive surface energy among the three catalysts, displays an increased diphenyl ether conversion, compared to the other two catalysts. The other two catalysts on the other hand, display similar diphenyl ether conversion, which is in good agreement with their comparable dispersive surface energies. The diphenyl ether conversion using the $\text{Ni}_2\text{P}/\text{SiO}_2\text{-20BTBSB}$ catalyst, which was found to be $84\pm 4\%$, is significantly higher compared to the other two catalysts, whereas in the case of $\text{Ni}_2\text{P}/\text{SiO}_2\text{-TEOS}$ the diphenyl ether conversion was found to be $40\pm 7\%$, and $49\pm 1\%$, in the case of the $\text{Ni}_2\text{P}/\text{SiO}_2\text{-50MTES}$ catalyst (Figure 5b). Considering the product distributions, cyclohexane was the primary product of the reaction, when $\text{Ni}_2\text{P}/\text{SiO}_2\text{-20BTBSB}$ was used with a selectivity of $59\pm 4\%$ compared to a benzene selectivity of $40\pm 4\%$. For the other two catalysts, benzene was found as the main product, with selectivity values of approximately 50%, and cyclohexane with ca. 40% selectivity.

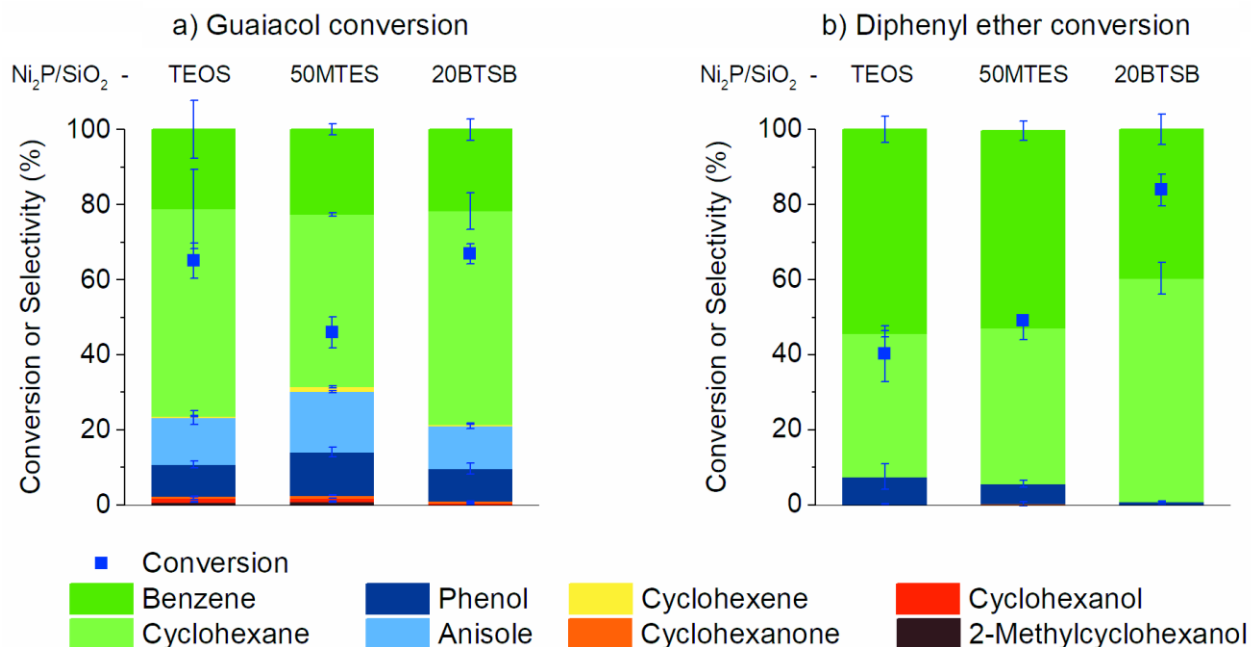


Figure 5 a) HDO of guaiacol using $\text{Ni}_2\text{P}/\text{SiO}_2$ -TEOS, $\text{Ni}_2\text{P}/\text{SiO}_2$ -50MTES and $\text{Ni}_2\text{P}/\text{SiO}_2$ -20BTBS catalysts. Reaction conditions: catalyst (50 mg), guaiacol (5 mmol), *n*-octane (9.5 mL), 295 °C, 5 MPa H_2 , 3 h; b) HDO of diphenyl ether using $\text{Ni}_2\text{P}/\text{SiO}_2$ -TEOS, $\text{Ni}_2\text{P}/\text{SiO}_2$ -50MTES and $\text{Ni}_2\text{P}/\text{SiO}_2$ -20BTBS. Reaction conditions: catalyst (50 mg), diphenyl ether (2.5 mmol), *n*-octane (2.5 mmol), 295 °C, 5 MPa H_2 , 6 h. All reactions were performed as triplicates.

These results show how the modification of $\text{Ni}_2\text{P}/\text{SiO}_2$ catalysts with either alkyl or phenyl functions influences the affinity of the catalyst towards either polar or nonpolar bio-oil parts. Evidently, the affinity towards polar compounds, characterized by the free energy of methanol adsorption, is lowered by incorporation of alkyl functional groups into $\text{Ni}_2\text{P}/\text{SiO}_2$, while this was not the case when phenyl groups were incorporated. Moreover, the presence of phenyl groups also intensified the interactions with the less polar substrate diphenyl ether, shown by the higher dispersive surface energy, resulting in a higher conversion for the $\text{Ni}_2\text{P}/\text{SiO}_2$ -20BTBS catalyst compared to the other two catalysts.

Implications of support polarity for catalyst stability

Besides conversion, catalyst stability is another crucial parameter to assess the performance of Ni_2P catalyst phase, because these are known to deactivate in the presence of water via oxidation of the active phase.²⁶ To explore the influence of modifying $\text{Ni}_2\text{P}/\text{SiO}_2$ catalysts with different types and amounts of organic functional groups on the stability of the Ni_2P phase, recycling experiments were performed. The results are presented in Figure 6, for the $\text{Ni}_2\text{P}/\text{SiO}_2$ -TEOS and $\text{Ni}_2\text{P}/\text{SiO}_2$ -50MTES catalysts, the first run was reproduced four times, the second run three times and the third run two times (only in the case of the $\text{Ni}_2\text{P}/\text{SiO}_2$ -50MTES catalyst). The error bars in Figure 6 indicate that the spread of the conversion and yield is within the range 5-12%.

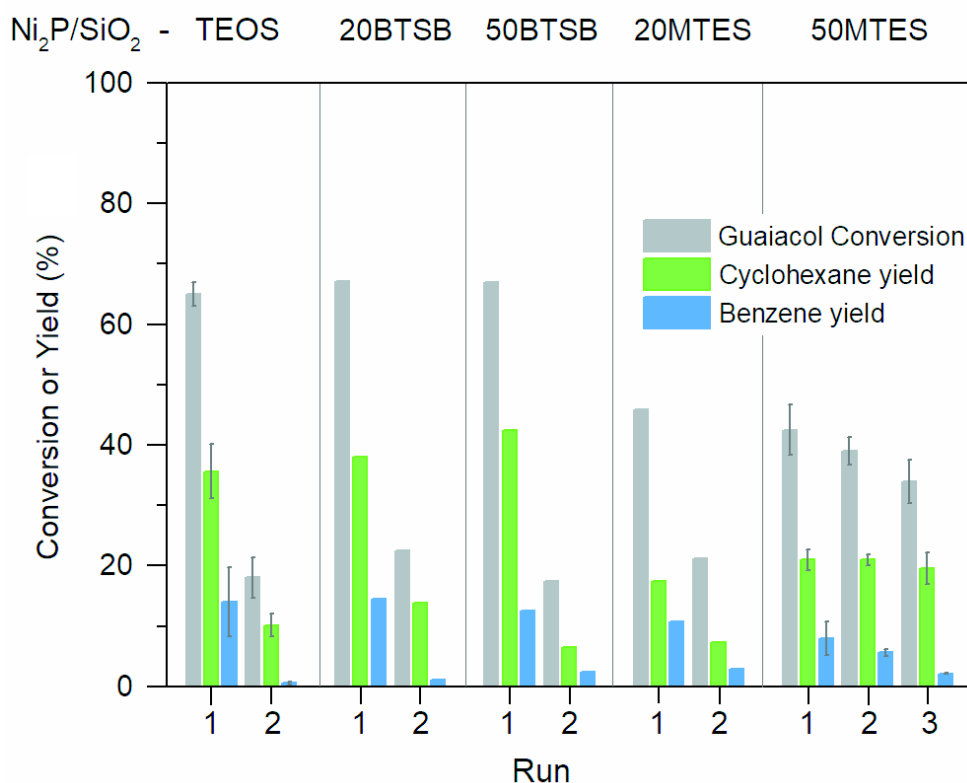


Figure 6 Guaiacol recycling experiments using the $\text{Ni}_2\text{P}/\text{SiO}_2$ -TEOS, $\text{Ni}_2\text{P}/\text{SiO}_2$ -20BTB, $\text{Ni}_2\text{P}/\text{SiO}_2$ -50BTB, $\text{Ni}_2\text{P}/\text{SiO}_2$ -20MTES and $\text{Ni}_2\text{P}/\text{SiO}_2$ -50MTES catalysts. Reaction conditions: catalyst (50 mg), guaiacol (5 mmol), *n*-octane (9.5 mL), 295 °C, 5 MPa H_2 , 3 h. For the $\text{Ni}_2\text{P}/\text{SiO}_2$ -TEOS and $\text{Ni}_2\text{P}/\text{SiO}_2$ -50MTES catalysts, the first run was repeated four times, the second run three times and the third run two times.

As expected from previous studies,²⁶ Ni₂P/SiO₂-TEOS catalyst strongly deactivated upon recycling. The conversion decreased from 59±12%, in the first run, to 18±3% in the second run (Figure 6). Strikingly, Ni₂P/SiO₂-20BSTB and Ni₂P/SiO₂-50BSTB, modified with phenyl groups, and Ni₂P/SiO₂-20MTES catalyst, also suffered from substantial deactivation after the first run. Consistently, Ni₂P/SiO₂-20BSTB, Ni₂P/SiO₂-50BSTB and Ni₂P/SiO₂-20MTES showed a deactivation profile similar to the Ni₂P/SiO₂-TEOS catalyst, in terms of decreasing conversion and decreasing yield of deoxygenated products (Figure 6). In stark contrast, the cyclohexane yield for Ni₂P/SiO₂-50MTES catalyst remained around 20% throughout the three recycling runs. Interestingly, the benzene yield also decreased for this catalyst from 8±3% down to 2.0±0.1% from the first to the third run. Most importantly, among the five investigated catalysts, only Ni₂P/SiO₂-50MTES catalyst presented an improved stability. Indeed, only a slight decrease in the conversion from 43±4%, in the first run, to 39±2% in the second run, and 34±4% in the third run was observed.

The improved stability of the Ni₂P/SiO₂-50MTES catalyst was further corroborated by HR-TEM results. Figure 7 compares HR-TEM images of the fresh Ni₂P/SiO₂-TEOS (Figure 7a) and Ni₂P/SiO₂-50MTES (Figure 7b) catalysts to the catalysts after one HDO reaction. In the case of the Ni₂P/SiO₂-TEOS catalyst, the catalyst after one reaction visually differs significantly from the fresh catalyst. There are new support domains formed in the material, which seem to be amorphous and were not present on the fresh catalyst (indicated by yellow arrows in Figure 7a). In comparison, the TEM image of Ni₂P/SiO₂-50MTES catalyst after one reaction (Figure 7b) does not differ substantially from the fresh Ni₂P/SiO₂-50MTES catalyst.

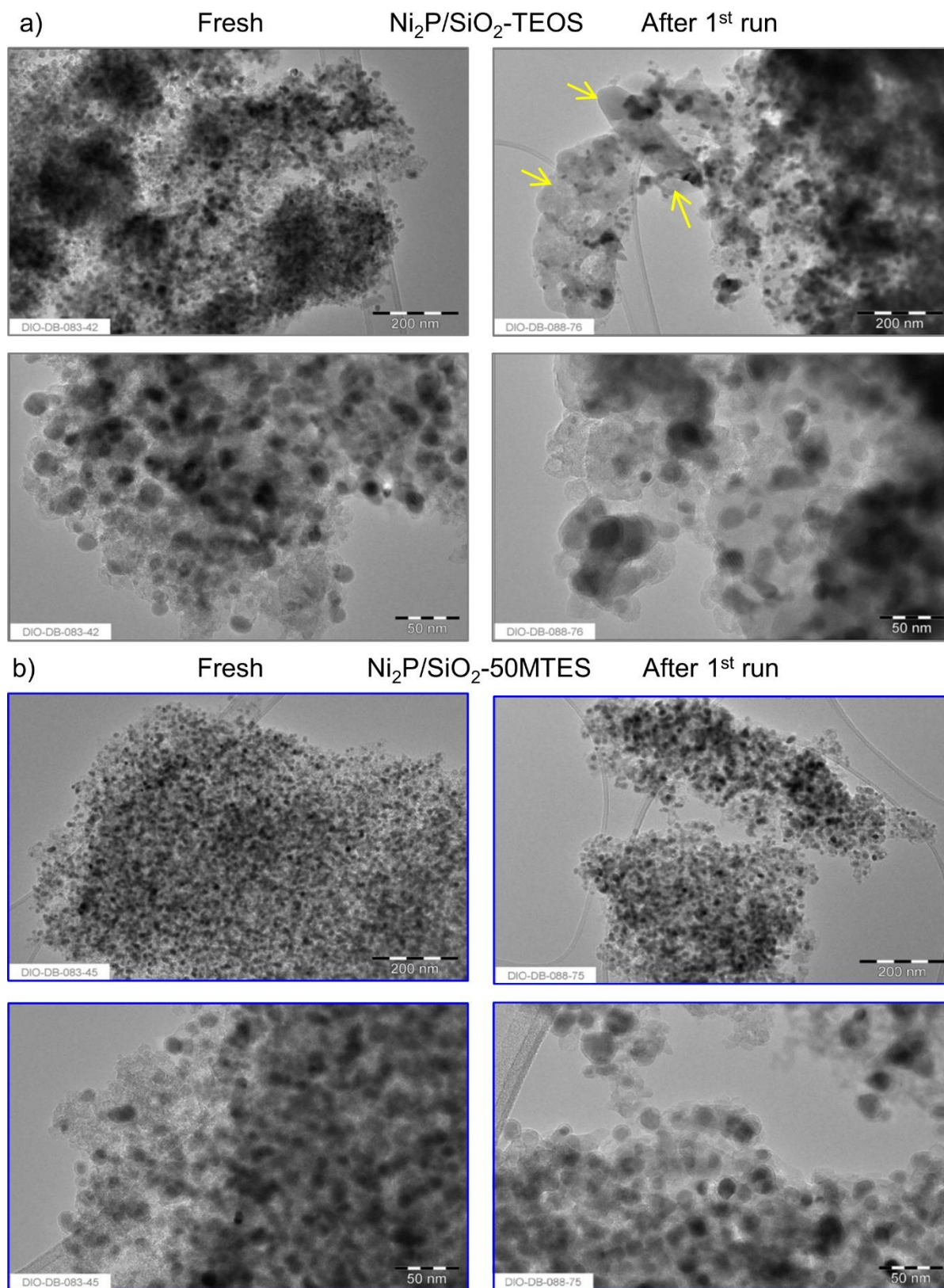


Figure 7 TEM images of the fresh and recycled $\text{Ni}_2\text{P}/\text{SiO}_2\text{-TEOS}$ catalysts (a) and $\text{Ni}_2\text{P}/\text{SiO}_2\text{-50MTES}$ (b). Yellow arrows indicate the new domains formed on the catalyst during recycling.

XRD analysis of the recycled catalysts after one reaction provides additional pieces of evidence for the statement that only the $\text{Ni}_2\text{P}/\text{SiO}_2\text{-50MTES}$ catalyst repels water strongly enough to prevent catalyst deactivation (Figure 8). Clearly, comparing the XRD pattern of the fresh $\text{Ni}_2\text{P}/\text{SiO}_2\text{-TEOS}$ catalyst (Figure 8a) to the XRD pattern of the $\text{Ni}_2\text{P}/\text{SiO}_2\text{-TEOS}$ catalyst after one reaction (Figure 8b) revealed significant differences between the two. Besides the reflections for Ni_2P (▲), also those for the Ni_{12}P_5 phase (●), a more P lean phase compared to Ni_2P , and for the NiP_2 (■) phase were found, which is richer in P compared to Ni_2P . Also the XRD patterns of the $\text{Ni}_2\text{P}/\text{SiO}_2\text{-20BSTB}$ (Figure 8c) and $\text{Ni}_2\text{P}/\text{SiO}_2\text{-50BSTB}$ (Figure 8d) catalysts after one reaction display new reflections which can be related to the Ni_{12}P_5 phase. Moreover, in these cases, the intensity of the reflections is much lower, which could indicate a decrease in the crystallinity. In contrast, the XRD patterns of the $\text{Ni}_2\text{P}/\text{SiO}_2\text{-20MTES}$ (Figure 8e) and $\text{Ni}_2\text{P}/\text{SiO}_2\text{-50MTES}$ (Figure 8f) catalysts, after one run, still resembled the pattern of a fresh $\text{Ni}_2\text{P}/\text{SiO}_2$ catalyst. XRD results demonstrate that the MTES modified catalysts to be less affected by water during recycling, compared to the other catalysts. Nonetheless, very low-intensity reflections for the Ni_{12}P_5 phase are observed. Even though the XRD pattern of the spent $\text{Ni}_2\text{P}/\text{SiO}_2\text{-20MTES}$ catalyst still resembled the Ni_2P phase, recycling experiments showed that this catalyst presents decreased performance.

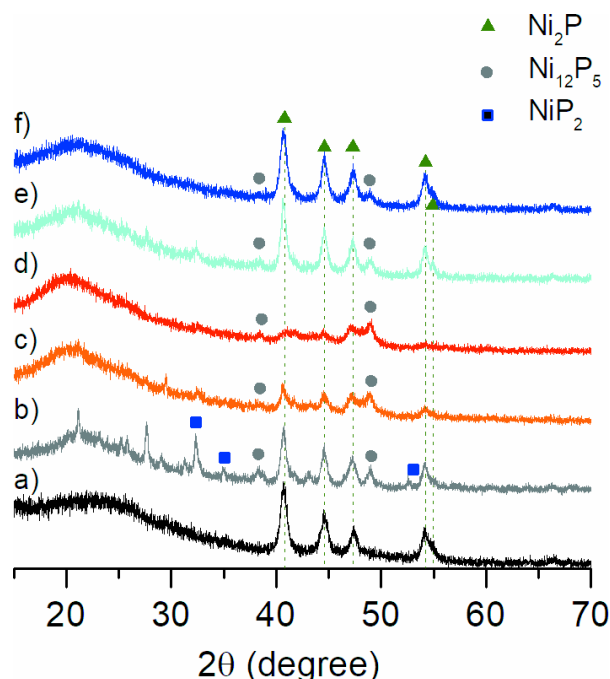


Figure 8 a) XRD of the fresh $\text{Ni}_2\text{P}/\text{SiO}_2\text{-TEOS}$ catalyst b) the $\text{Ni}_2\text{P}/\text{SiO}_2\text{-TEOS}$ catalyst after first run, c) the $\text{Ni}_2\text{P}/\text{SiO}_2\text{-20BTSB}$ catalyst after the first run, d) the $\text{Ni}_2\text{P}/\text{SiO}_2\text{-50BTSB}$ catalyst after first run, e) the $\text{Ni}_2\text{P}/\text{SiO}_2\text{-20MTES}$ after first run, f) the $\text{Ni}_2\text{P}/\text{SiO}_2\text{-50MTES}$ after the first run.

It has previously been reported that SiO_2 supported Ni_2P catalysts deactivate faster during HDO than Ni_2P supported on other supports, due to the hydrophilic nature of silica.²⁶ Through the hydrophilic nature of the support, water adsorption and the hydration of the catalyst surface is promoted and, therefore, the oxidation of the active phase by water is accelerated. To explain the deactivation behavior of the different catalysts, the affinity of these towards water was characterized, using specific surface energies ($\gamma_{\text{S}}^{\text{SP}}$), derived from polar probe interactions and the free energies of methanol adsorption ($-\Delta G_{\text{ads}}^{\text{SP}}(\text{MeOH})$).

Considering the $\gamma_{\text{S}}^{\text{SP}}$ (Figure 9), the $\text{Ni}_2\text{P}/\text{SiO}_2\text{-20BSTB}$ displays the highest value of 257 mJ/m^2 , which decreases for the $\text{Ni}_2\text{P}/\text{SiO}_2\text{-50BSTB}$ catalyst down to 193 mJ/m^2 , in line with the increased amount of phenyl groups. Changing the organic function from phenyl to methyl, the $\gamma_{\text{S}}^{\text{SP}}$ decreases to 121 mJ/m^2 for the $\text{Ni}_2\text{P}/\text{SiO}_2\text{-20MTES}$ catalyst. For the $\text{Ni}_2\text{P}/\text{SiO}_2\text{-50MTES}$ catalyst,

this value further decreases to 81 mJ/m², consistent with the increased number of methyl groups. The γ_S^{SP} for Ni₂P/SiO₂-TEOS, however, was found to be 89 mJ/m² and is comparable to the one of Ni₂P/SiO₂-50MTES catalyst. Nonetheless, the free energy of methanol adsorption, which can be interpreted as an indicator for the affinity of the catalyst towards water, is 15.0 kJ mol⁻¹ for the Ni₂P/SiO₂-TEOS catalyst.²¹ This is comparably high, in contrast to the value of the Ni₂P/SiO₂-50MTES catalyst, which displays a free energy of methanol adsorption of only 10.7 kJ mol⁻¹, which is the lowest value among all the investigated catalysts (Figure 9). In line with the observed deactivation of the Ni₂P/SiO₂-20MTES catalyst during recycling, also this catalyst displays a higher free energy of methanol adsorption (13.1 kJ mol⁻¹) than the Ni₂P/SiO₂-50MTES catalyst. Consistently, the free energies of methanol adsorption for the phenyl modified catalysts, which also deactivated during recycling, were found to be 13.9 kJ mol⁻¹ and 17.8 kJ mol⁻¹ for the Ni₂P/SiO₂-50BSTB and the Ni₂P/SiO₂-20BSTB catalyst, respectively. The higher polar character of phenyl modified catalysts can be explained in terms of the ability of phenyl groups to interact with polar compounds via π - π interactions as well as via weak hydrogen bonding interactions, which is well known from gas and liquid chromatography.⁴⁵ These results suggest that the interactions between water present under reactions conditions and the catalyst can be correlated with $(-\Delta G_{ads}^{SP}(\text{MeOH}))$, and must be decreased below a certain threshold to prevent the catalyst from immediate deactivation. In the case of methyl group modified catalysts, this threshold lies somewhere between a R:TEOS ratio of 0.2 and 0.5. Overall, these results highlight how proper adjustment of the catalyst polarity can help to alleviate the deactivation of Ni₂P/SiO₂ catalysts.

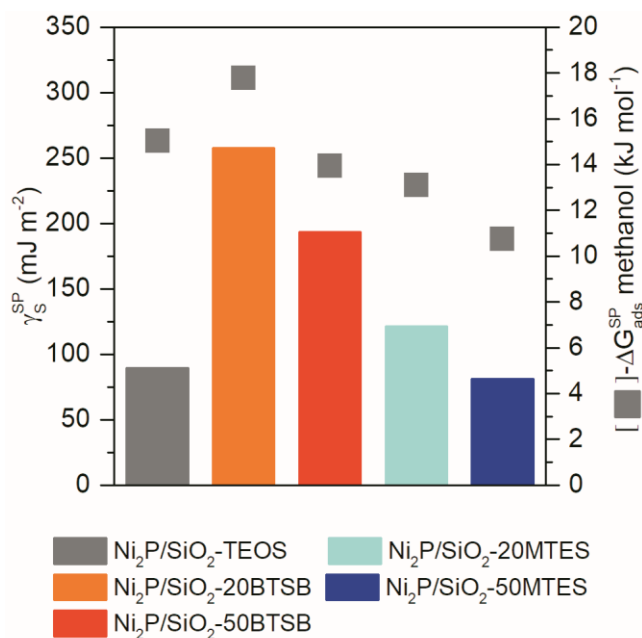


Figure 9 Specific surface energy (γ_s^{SP} , represented by the colored bars) and free energy of methanol adsorption ($-\Delta G_{ads}^{SP}(\text{MeOH})$, indicated by squares in gray color) for the catalysts tested in the recycling experiments.

Conclusions

In this work, the influence of the catalyst polarity on the activity and stability of HDO catalysts was investigated, using a Ni₂P/SiO₂ catalyst as a model catalyst. Among the differently modified catalysts, only the catalyst modified with methyl functions, having an initial R:Si ratio of 0.5, did not show immediate deactivation during guaiacol HDO recycling experiments. Consistently, this catalyst also displayed the lowest free energy of methanol adsorption. Strikingly, phenyl groups are not suitable to stabilize the catalyst against water deactivation. Apparently, these groups may establish polar π - π interactions, uncovering the support surface against water. Our results demonstrate the modification of silica with methylsilane groups to be more suitable for improving the stability of HDO catalysts against the deleterious effect of water under reaction conditions. Apparently, there is a threshold, which is reached with increasing the amount of alkylsilane

modifier, above which the affinity of the catalyst towards water becomes so low, that the active phase does not deactivate immediately under the HDO process conditions. However, it was also shown that modification of the polar properties of the catalysts additionally affects the catalytic activity. Thus, the $\text{Ni}_2\text{P}/\text{SiO}_2\text{-50MTES}$ showed a lower activity for guaiacol HDO, which is an example of a polar bio-oil compound, most likely due to the lower affinity of this catalyst towards polar substances, compared to the $\text{Ni}_2\text{P}/\text{SiO}_2\text{-TEOS}$ and $\text{Ni}_2\text{P}/\text{SiO}_2\text{-20BSTB}$ catalysts. Finally, diphenyl ether HDO was performed as a model reaction for a less polar constituent of pyrolysis oils, showing that the $\text{Ni}_2\text{P}/\text{SiO}_2\text{-TEOS}$ and $\text{Ni}_2\text{P}/\text{SiO}_2\text{-50MTES}$ catalysts displayed comparable conversions, while the $\text{Ni}_2\text{P}/\text{SiO}_2\text{-20BSTB}$ catalyst had a higher conversion. In agreement with this, $\text{Ni}_2\text{P}/\text{SiO}_2\text{-20BSTB}$ also displayed the highest dispersive surface energy, while the other two catalysts exhibited similar dispersive surface energies. This work thus highlights, how the fine-tuning of the catalyst polarity can be employed for improving stability and activity of HDO catalysts, which primarily deactivate by oxidation through water, as exemplified by using a $\text{Ni}_2\text{P}/\text{SiO}_2$ catalyst.

Acknowledgments

This work was also conducted within the framework of the CASCATBEL project funded by the European Commission (Grant Agreement No.604307). R.R. acknowledges the financial support provided by the ERC Consolidator Grant (LIGNINFIRST, Project Number: 725762). KW acknowledges the Royal Society for the award of an Industry Fellowship, and the EPSRC under grant (EP/K000616/2) for financial support to JCM. The authors are grateful Mr Bernd Spliethoff for HRTEM analyses.

Experimental section

Materials: nickel(II) nitrate hexahydrate ($\geq 97.0\%$), tetraethyl orthosilicate ($\geq 99.0\%$), triethoxymethylsilane (99%), triethoxyethylsilane (96%), triethoxyphenylsilane (98%), 1,4-(bistriethoxysilyl)benzene (96%), triethoxyoctylsilane (≥ 97.5), sodium hypophosphite (anhydrous), dichloromethane ($\geq 99\%$), *n*-octane ($>99.5\%$), ethanol (≥ 99.8), guaiacol ($>99\%$), diphenyl ether (99%), phenol ($>99.5\%$) and *n*-hexadecane (99%) were purchased from Sigma Aldrich and used without further purification. Citric acid monohydrate (99.5%) was purchased from VWR.

Preparation of Ni/SiO₂: In a typical synthesis, citric acid monohydrate ('CA') was first dissolved in ethanol at 50 °C in a 50-mL polypropylene container. After cooling down to room temperature, nickel nitrate hexahydrate and nitric acid were added to the citric acid solution. The solution was stirred until a clear green colored solution was obtained. Afterwards, TEOS was added dropwise to the solution under magnetic stirring for 1 h. Next, the open container was left for 3 days at 25 °C, followed by drying at 50 °C for other additional three days. The various ratios of organosilane were set to Si:Ni(NO₃)₂:CA:R:H₂O:EtOH = 1:0.5:1:R:4:6. R represents the molar amount of organic function in the case of organohybrid silica supports, which were prepared by using a mixture of organosilane and TEOS instead of neat TEOS. For instance, for Ni/SiO₂-TEOS, citric acid monohydrate (4.74g, 22.6 mmol), ethanol (6.23 g, 135 mmol), Ni(NO₃)₂·6H₂O (3.28 g, 11.3 mmol), HNO₃ (1.6252 g), TEOS (4.71 g, 22.6 mmol). The molar amount of H₂O is given as the amount of H₂O present in a 0.25 mol L⁻¹ HNO₃ solution. For all the gels, the total quantity of silicon was kept constant. To obtain the Ni/SiO₂ precursors, the gels were first heated to 170 °C for 1.5 h and sequentially to 400 °C for 2 h using a heating ramp of 100 °C h⁻¹ under an Ar-flow. The Ni/SiO₂ catalyst prepared using only TEOS as the silicon source presents a 33 wt% nominal Ni loading.

Phosphidation of Ni/SiO₂ precursors: Ni/SiO₂ precursors were converted into Ni₂P/organohybrid-SiO₂ catalysts using NaH₂PO₂ as the P source ($2 \text{ NaH}_2\text{PO}_2(\text{s}) \rightarrow \text{Na}_2\text{HPO}_4(\text{s}) + \text{PH}_3(\text{g})$). For the reaction, NaH₂PO₂ (0.8 g) and Ni/SiO₂ precursor (0.1 g) were placed separately (approximately 1 cm distance between the powders) in a crucible (Scheme 1). NaH₂PO₂ was located on the inlet Ar-flow side, while Ni/SiO₂ on the outlet flow side. The crucible was placed in a tube furnace. Next, the system was flushed with Ar for 0.5 h and then heated to 300 °C and kept at this temperature for 1 h.

Catalyst characterization

Textural characterization: N₂-adsorption-desorption isotherms of Ni₂P/SiO₂ catalysts were measured at -196 °C on a Micromeritics 3-Flex physisorption instrument. On the instrument, the samples were degassed under vacuum (1.3 mbar) at 120 °C for 3 h. Specific surface area was calculated by using the BET method in the relative pressure range from 0.05 to 0.25. For the determination of the pore size distribution by the BJH method, the adsorption branch of the isotherm was used.

Attenuated Total Reflectance Infrared Spectroscopy (ATR-IR): Spectra were collected on a Nicolet Magna 560 FTIR spectrometer using 64 scans of 4000–800 cm⁻¹ with a resolution of 4 cm⁻¹. The instrument was equipped with an MCT-A detector, cooled by liquid nitrogen and a Diamond ATR-IR crystal.

X-ray powder diffraction (XRD): XRD patterns were obtained on an STOE Stadi P transmission X-ray diffractometer using CuKα₁ radiation ($\lambda = 1.5405 \text{ \AA}$) operated in transmission mode at 40 kV, 40 mA. The patterns were collected in the 2θ range from 15 to 70°, with a step size of 0.5° and counting time of 30 s. Samples were placed in a glass capillary with a diameter of 7 mm.

Transmission electron microscopy (TEM): For the measurements, the solid samples were deposited on a lacey carbon copper grid. Images were taken on a Hitachi HF-2000 FE transmission electron microscope operating at a voltage of 200 kV.

Inverse gas chromatography (IGC): Experiments to determine the surface polarity of NiP₂/SiO₂ catalysts were carried out on an automated IGC system (Surface Measurement Systems Ltd. - SMS) with IGC controller v1.8 software. A catalyst sample (0.0150 g) was packed into a glass column (300 mm × 2 mm i.d.) by tapping until no cracks or hollows were present in the powder bed. The columns were loosely stoppered with glass wool in both ends. The powder filled columns were outgassed under He for 2 h at 120 °C to remove adsorbed water. Probe molecules were carried into the column with a He flow of 10 mL min⁻¹. Retention times were recorded by a flame ionization detector (FID). *n*-Heptane, *n*-octane, *n*-nonane, and *n*-decane were used as nonpolar probe molecules, whereas methanol, acetonitrile, ethyl acetate, and dichloromethane as polar probes. The dead volume, the retention volume if there is no interaction between the probe and solid, was calculated based on the elution time of methane, which was run at a concentration of 0.1 *p/p*₀, where *p* is the partial pressure, and *p*₀ is the saturation pressure. The four *n*-alkanes were used to determine the dispersive surface energy (γ_S^D), and the four polar probes were used to determine the specific surface energy (polar interactions). Due to the analysis difficulty, as FID is not sensitive to water, methanol is selected as probe to measure the free energy of adsorption.

The interaction energy of a solid with a gas (γ_S) is equivalent to the sum of the dispersive (γ_S^D) and specific (γ_S^{SP}) surface energies:

$$\gamma_S = \gamma_S^D + \gamma_S^{SP} \quad (1)$$

To determine the dispersive part of the total surface energy, a homologous series of *n*-alkanes is studied, using IGC. In this case, it is assumed that these interact only via dispersive forces with the material surface. The net retention volume (*V_N*) for *n*-alkanes can be obtained according to:

$$V_N = \frac{T}{273.15} (t_r - t_0) F j \quad (2)$$

where T is the column temperature, t_r is the retention time of the probe molecule, t_0 is the dead retention time of methane, F is the carrier gas flow rate and j is the James-Martin correction factor, to correct the pressure drop along the packing of the column. The correction factor j can be obtained according to (3) where p is equal to the inlet pressure divided by the outlet pressure:

$$j = \frac{3}{2} \left(\frac{p^2 - 1}{p^3 - 1} \right) \quad (3)$$

V_N is related to the free energy of adsorption according to:

$$\Delta G_{ads} = -RT \ln(V_N) + C \quad (4)$$

where R is the gas constant, T is column temperature, V_N the net retention volume and C a constant depending on the chosen reference state. Moreover, the free energy is related to the work of adhesion W_a according to:

$$\Delta G_{ads} = N_A a W_a \quad (5)$$

where N_A is the Avogadro constant and a cross-sectional area of the adsorbate. W_a can also be formulated as:

$$W_a = 2\sqrt{\gamma_S^D \gamma_L^D} \quad (6)$$

where γ_L^D is the surface tension of the liquid probe molecule. Combining (4), (5) and (6) leads to:

$$RT \ln V_N = 2N_A a \sqrt{\gamma_S^D \gamma_L^D} + C \quad (7)$$

From this equation, γ_S^D can be obtained from the slope of a plot of $RT\ln V_N$ against $a\sqrt{\gamma_L^D}$. The specific interactions can be determined by calculating the difference of $RT\ln V_N$ for a polar probe molecule, e.g. methanol, dichloromethane and ethyl acetate to the plot of $RT\ln V_N$ against $a\sqrt{\gamma_L^D}$ for the series of homologous of *n*-alkanes.^{18, 46-49}

Horizontal microscope: pictures of the catalysts in contact with a water droplet were made using a horizontal Nikon SMZ-ZT light microscope. For the pictures, the catalyst powder was placed on a glass carrier, and water (8 μ L) was dropped onto the catalyst.

Catalytic tests:

HDO reactions: For a standard experiment, the substrate (5 mmol in the case of guaiacol and 2.5 mmol in the case of diphenyl ether) was placed into a quartz inlet together with *n*-octane (9.5 mL, solvent), *n*-hexadecane (internal standard for GC, 100 mg) and catalyst (50 mg). The reactions were then performed using a 45-mL autoclave at 5 MPa (measured at r.t.) of hydrogen pressure for 3 h, respectively 6 h in the case of biphenyl ether at 295 °C. The reaction time was measured right after inserting the autoclave into the preheated hot metal mold. Afterwards, the reactor was placed into an ice-bath. The resulting reaction mixture was homogenized by adding dichloromethane. Prior to offline GC analysis, the reaction mixture was dried using Na₂SO₄ and filtered afterwards.

Product analysis: The samples were analyzed by GC using an Agilent 6850 Network gas chromatograph, equipped with an Agilent HP-INNOWax column. The peaks were identified by GC-MS and the comparison of the retention times of standards. The injector temperature was 350 °C. The temperature program started with an isothermal step at 35 °C. Next, the temperature was increased from 35 to 90 °C at a rate of 10 °C min⁻¹ and kept at this temperature for 1 minute. Subsequently, the temperature was increased at 10 °C min⁻¹ to 150 °C. Afterwards, the temperature was increased to 250 °C with a heating ramp of 50 °C min⁻¹ and kept at this temperature for 2 min. Quantification was performed from the integration of GC peaks.

Typically, since only the ring products were identified, the ring balance was used to control the mass balance in this study. The ring balances were between 90 and 104%, and calculated product amounts have been normalized to 100%. The conversion, selectivity and 'C₆-ring balance' were determined according to the following equations:

$$\begin{aligned} \text{Conversion} &= \frac{n_{\text{substrate}}^{t=0} - n_{\text{substrate}}^{t=t_i}}{n_{\text{substrate}}^{t=0}} \times 100\% \\ \text{Selectivity} &= \frac{n_{\text{product}}^{t=t_i}}{n_{\text{substrate}}^{t=0} - n_{\text{substrate}}^{t=t_i}} \times 100\% \\ \text{Ring balance} &= \frac{\sum n_{\text{product}}^{t=t_i} + n_{\text{substrate}}^{t=t_i}}{n_{\text{substrate}}^{t=0}} \times 100\% \end{aligned}$$

where, $n_{\text{substrate}}^{t=0}$ is the initial quantity of substrate (mol), $n_{\text{substrate}}^{t=t_i}$ the quantity of substrate at a time t_i , $n_{\text{product}}^{t=t_i}$ the quantity of product formed at t_i .

References

1. J. C. Serrano-Ruiz and J. A. Dumesic, *Energy Environ. Sci.*, 2011, **4**, 83-99.
2. R. Rinaldi, R. Jastrzebski, M. T. Clough, J. Ralph, M. Kennema, P. C. A. Bruijninx and B. M. Weckhuysen, *Angew. Chem. Int. Ed.*, 2016, **55**, 8164-8215.
3. G. W. Huber, S. Iborra and A. Corma, *Chem. Rev.*, 2006, **106**, 4044-4098.
4. A. V. Bridgwater, *Biomass Bioenerg.*, 2012, **38**, 68-94.
5. A. H. Van Pelt, O. A. Simakova, S. M. Schimming, J. L. Ewbank, G. S. Foo, E. A. Pidko, E. J. Hensen and C. Sievers, *Carbon*, 2014, **77**, 143-154.
6. A. L. Jongerius, J. R. Copeland, G. S. Foo, J. P. Hofmann, P. C. Bruijninx, C. Sievers and B. M. Weckhuysen, *ACS Catalysis*, 2013, **3**, 464-473.

7. R. M. Ravenelle, J. R. Copeland, W.-G. Kim, J. C. Crittenden and C. Sievers, *ACS Catalysis*, 2011, **1**, 552-561.
8. R. M. Ravenelle, F. Schüßler, A. D'Amico, N. Danilina, J. A. Van Bokhoven, J. A. Lercher, C. W. Jones and C. Sievers, *The Journal of Physical Chemistry C*, 2010, **114**, 19582-19595.
9. S. K. Wu, P. C. Lai, Y. C. Lin, H. P. Wan, H. T. Lee and Y. H. Chang, *ACS Sustain. Chem. Eng.*, 2013, **1**, 349-358.
10. D. A. Ruddy, J. A. Schaidle, J. R. Ferrell, J. Wang, L. Moens and J. E. Hensley, *Green Chem.*, 2014, **16**, 454-490.
11. E. Laurent and B. Delmon, *J. Catal.*, 1994, **146**, 281-291.
12. W. Y. Wang, P. L. Liu, K. Wu, S. Tan, W. S. Li and Y. Q. Yang, *Green Chem.*, 2016, **18**, 984-988.
13. H. Song, J. Gong, H. L. Song and F. Li, *Appl. Catal., A*, 2015, **505**, 267-275.
14. L. Wang and F. S. Xiao, *ChemCatChem*, 2014, **6**, 3048-3052.
15. S. Klein and W. F. Maier, *Angew. Chem. Int. Ed.*, 1996, **35**, 2230-2233.
16. A. Corma, P. Esteve and A. Martinez, *J. Catal.*, 1996, **161**, 11-19.
17. K. Nakatsuka, K. Mori, S. Okada, S. Ikurumi, T. Kamegawa and H. Yamashita, *Chem.-Eur. J.*, 2014, **20**, 8348-8354.
18. C. Pirez, A. F. Lee, C. Jones and K. Wilson, *Catal. Today*, 2014, **234**, 167-173.
19. A. Mobaraki, B. Movassagh and B. Karimi, *Appl. Catal., A*, 2014, **472**, 123-133.
20. Y. Dai, S. J. Liu and N. F. Zheng, *J. Am. Chem. Soc.*, 2014, **136**, 5583-5586.
21. G. Huang, Q. H. Yang, Q. Xu, S. H. Yu and H. L. Jiang, *Angew. Chem. Int. Ed.*, 2016, **55**, 7379-7383.
22. J. D. Lin, Q. Y. Bi, L. Tao, T. Jiang, Y. M. Liu, H. Y. He, Y. Cao and Y. D. Wang, *ACS Catal.*, 2017, **7**, 1720-1727.

23. L. Wang, H. Wang, F. J. Liu, A. M. Zheng, J. Zhang, Q. Sun, J. P. Lewis, L. F. Zhu, X. J. Meng and F. S. Xiao, *ChemSusChem*, 2014, **7**, 402-406.
24. P. A. Zapata, J. Faria, M. P. Ruiz, R. E. Jentoft and D. E. Resasco, *J. Am. Chem. Soc.*, 2012, **134**, 8570-8578.
25. J. C. Manayil, V. C. dos Santos, F. C. Jentoft, M. Granollers Mesa, A. F. Lee and K. Wilson, *ChemCatChem*, 2017.
26. J. S. Moon and Y. K. Lee, *Top. Catal.*, 2015, **58**, 211-218.
27. K. L. Li, R. J. Wang and J. X. Chen, *Energy Fuels*, 2011, **25**, 854-863.
28. R. Takahashi, S. Sato, T. Sodesawa, M. Suzuki and N. Ichikuni, *Microporous Mesoporous Mater.*, 2003, **66**, 197-208.
29. R. Takahashi, S. Sato, T. Sodesawa, M. Kawakita and K. Ogura, *J. Phys. Chem. B*, 2000, **104**, 12184-12191.
30. F. Hoffmann, M. Cornelius, J. Morell and M. Froba, *Angew. Chem. Int. Ed.*, 2006, **45**, 3216-3251.
31. A. L. Smith, *Spectrochim. Acta*, 1960, **16**, 87-105.
32. C. A. Lanziano, S. F. Moya, D. H. Barrett, R. Guirardello, F. de Souto da Silva, R. Rinaldi and C. B. Rodella, *ChemSusChem*, 2018.
33. I. Barin, *Thermochemical Data of Pure Substances, Third Edition*, 1995, 1-20.
34. B. M. Abu-Zied and A. M. Asiri, *Thermochim. Acta*, 2017, **649**, 54-62.
35. W. Jang, Y. Lu, W. Hwang, C. Dong, P. Hsieh, C. Chen, T. Chan and J. Lee, *EPL*, 2011, **96**, 37009.
36. S. S. A. Syed-Hassan and C.-Z. Li, *Applied Catalysis A: General*, 2011, **398**, 187-194.
37. D. Mohan, C. U. Pittman and P. H. Steele, *Energy Fuels*, 2006, **20**, 848-889.
38. H. Wang, J. Male and Y. Wang, *ACS Catal.*, 2013, **3**, 1047-1070.

39. M. Rückriem, A. Inayat, D. Enke, R. Gläser, W.-D. Einicke and R. Rockmann, *Colloids and Surfaces A: Physicochemical and Engineering Aspects*, 2010, **357**, 21-26.
40. S. C. Das and P. J. Stewart, *J Pharm Pharmacol*, 2012, **64**, 1337-1348.
41. E. Papirer, E. Brendle, F. Ozil and H. Balard, *Carbon*, 1999, **37**, 1265-1274.
42. X. Zhang, D. Yang, P. Xu, C. Wang and Q. Du, *J Mater Sci*, 2007, **42**, 7069-7075.
43. C. Pirez, A. F. Lee, C. Jones and K. Wilson, *Catal. Today*, 2014, **234**, 167-173.
44. D. F. Steele, R. C. Moreton, J. N. Staniforth, P. M. Young, M. J. Tobyn and S. Edge, *The AAPS journal*, 2008, **10**, 494-503.
45. B. Kolb, in *Gaschromatographie in Bildern: Eine Einführung*, John Wiley & Sons, 2012.
46. G. M. Dorris and D. G. Gray, *J. Colloid Interface Sci.*, 1980, **77**, 353-362.
47. S. Katz and D. G. Gray, *J. Colloid Interface Sci.*, 1981, **82**, 318-325.
48. J. Donnet, S. Park and H. Balard, *Chromatographia*, 1991, **31**, 434-440.
49. M. Rückriem, D. Enke and T. Hahn, *Microporous Mesoporous Mater.*, 2015, **209**, 99-104.

FULL PAPER

Let it rain. Herein, the dependence of stability and activity of $\text{Ni}_2\text{P}/\text{SiO}_2$ HDO catalysts on the support surface polarity is addressed in detail. The correlation between catalyst performance and support surface polarity indicates that, to prevent deactivation of the catalyst by water under reaction conditions, the affinity of the support towards polar substances must be decreased below a certain threshold value.



Michael Dierks, Zhengwen Cao, Jinesh C. Manayil, Jeganathan Akilavasan, Karen Wilson, Ferdi Schüth* and Roberto Rinaldi*

Page No. – Page No.

On the impact of hydrophobic organohybrid silicas on the stability of Ni_2P catalyst phase in the HDO of biophenols

Accepted Manuscript